The Astrophysical Journal, 1002:143 (7pp), 2026 May 10 https://doi.org/10.3847/1538-4357/ae5a8e

X-Ray Polarization from the Atoll 4U 1735−44 Suggests a Low Inclination

María Alejandra Díaz Teodori[1,2], Anna Bobrikova[1], Andrea Gnarini[3,4], Francesco Ursini[4], Sofia V. Forsblom[1], Juri Poutanen[1], Alexander Salganik[1], Stefano Bianchi[4], Fiamma Capitanio[5], Massimo Cocchi[6], Sergio Fabiani[5], Ruben Farinelli[7], Philip Kaaret[3], Jari J. E. Kajava[8], Giorgio Matt[4], Mason Ng[9,10,11], Swati Ravi[9], Paolo Soffitta[5], Antonella Tarana[5], and Silvia Zane[12]

[1] Department of Physics and Astronomy, FI-20014, University of Turku, Finland; alejandra.m.diaz@utu.fi
[2] Nordic Optical Telescope, Rambla José Ana Fernández, Pérez 7, E-38711 Breña Baja, Spain
[3] NASA Marshall Space Flight Center, Huntsville, AL 35812, USA
[4] Dipartimento di Matematica e Fisica, Università degli Studi Roma Tre, via della Vasca Navale 84, 00146 Roma, Italy
[5] INAF Istituto di Astrofisica e Planetologia Spaziali, Via del Fosso del Cavaliere 100, 00133 Roma, Italy
[6] INAF Osservatorio Astronomico di Cagliari, via della Scienza 5, I-09047, Selargius (CA), Italy
[7] INAF Osservatorio di Astrofisica e Scienza dello Spazio, Via P. Gobetti 101, 40129 Bologna, Italy
[8] Serco for the European Space Agency (ESA), European Space Astronomy Centre, Camino Bajo del Castillo s/n, E-28692 Villanueva de la Cañada, Madrid, Spain
[9] MIT Kavli Institute for Astrophysics and Space Research, Massachusetts Institute of Technology, 77 Massachusetts Avenue, Cambridge, MA 02139, USA
[10] Department of Physics, McGill University, 3600 rue University, Montréal, QC H3A 2T8, Canada
[11] Trottier Space Institute, McGill University, 3550 rue University, Montréal, QC H3A 2A7, Canada
[12] Mullard Space Science Laboratory, University College London, Holmbury St Mary, Dorking, Surrey RH5 6NT, UK
Received 2025 July 4; revised 2026 March 18; accepted 2026 March 31; published 2026 May 4

Abstract

X-ray polarimetry is a new tool capable of probing the geometry of accretion onto weakly magnetized neutron stars. Here we present the first X-ray spectropolarimetric results from coordinated observations of the atoll source 4U 1735−44, conducted with the Imaging X-ray Polarimetry Explorer (IXPE), Neutron Star Interior Composition Explorer, and Nuclear Spectroscopic Telescope Array. Over the 2–8 keV energy range, we obtained a marginal detection of polarization with the polarization degree of 1.4% ± 0.7% and polarization angle of −29° ± 14°, corresponding to a 3σ upper limit on the polarization degree of 3.5%. The best-fit model to describe the spectrum comprises a thermal component associated with the accretion disk, a Comptonized blackbody component, and a relativistic reflection component. From the reflection model, we infer a disk inclination of ∼40°. The spectroscopic and polarimetric properties of 4U 1735−44 are consistent with those observed in other atoll sources studied by IXPE, with its low polarization likely due to its low inclination.

Unified Astronomy Thesaurus concepts: Stellar accretion disks (1579); Neutron stars (1108); Low-mass x-ray binary stars (939); Spectropolarimetry (1973); Polarimetry (1278)

1. Introduction

Accreting weakly magnetized neutron stars (WMNSs) in low-mass X-ray binaries (LMXBs) are among the brightest X-ray sources in the sky and exhibit complex behavior that is not yet fully understood. They accrete mass via Roche-lobe overflow from a low-mass (typically $\leqslant 1\,M_{\odot}$) companion, forming an accretion disk (A. Bahramian & N. Degenaar 2024).

The spectrum of WMNSs is usually modeled by the sum of two components: a soft thermal component (<1 keV) associated with the accretion disk (N. I. Shakura & R. A. Sunyaev 1973), and a hard component resulting from Comptonization in a relatively cool plasma in the boundary layer (BL) between the disk and the neutron star (NS) surface (N. I. Shakura & R. A. Sunyaev 1988; R. Popham & R. Sunyaev 2001) or the spreading layer (SL) where the accreted material spreads to higher latitudes (N. A. Inogamov & R. A. Sunyaev 1999; V. Suleimanov & J. Poutanen 2006). In addition, X-ray illumination of the accretion disk can produce a reflection component with both continuum and line features, most notably an iron emission line at 6–7 keV. Furthermore, WMNSs can also display Type-I X-ray bursts, which are caused by thermonuclear explosions of the matter accreted from a companion onto the NS surface (see, e.g., W. H. G. Lewin et al. 1993).

Beyond these common characteristics, WMNSs have historically been classified into two main categories: *Z* and atoll sources (see, e.g., G. Hasinger & M. van der Klis 1989). This classification is based on the patterns these sources display in the color–color diagram (CCD) or the hardness–intensity diagram (HID), as well as their correlated spectral and timing properties. Atoll sources are characterized by a lower luminosity (10^{36}–10^{37} erg s^{-1}) compared to *Z* sources (10^{38} erg s^{-1}, near the Eddington luminosity).

Despite all the advances that have been made in studying the WMNS with spectroscopy and timing, many fundamental questions remain open. For instance, both the classification into *Z* and atoll sources and the state transitions of the sources lack physical explanations. The geometry of the region between the NS surface and the inner parts of the accretion disk also remains a mystery. In this context, polarimetry is a powerful tool to examine the geometry of the surroundings of compact objects. Polarimetric properties of the emission coming from different regions of the WMNS have been predicted by M. Dovčiak et al. (2008) and V. Loktev et al. (2022) for the disk, by I. I. Lapidus & R. A. Sunyaev (1985), A. Gnarini et al. (2022), R. Farinelli et al. (2024), and

A. Bobrikova et al. (2025) for the Comptonized component, and by G. Matt (1993) and J. Poutanen et al. (1996) for the reflected component.

Since the launch of the Imaging X-ray Polarimetry Explorer (IXPE; M. C. Weisskopf et al. 2022) in 2021 December, X-ray polarimetry has been actively used to study the geometry of various accreting compact objects. Only for the WMNSs, a dozen discoveries have been made. For instance, in the *Z*-source Cyg X-2 (R. Farinelli et al. 2023), the polarization of the Comptonized component was aligned with the jet, putting a constraint on the geometry of the boundary region. For the atoll sources GX 9+9, 4U 1820−303, and 4U 1624−49, a trend of a strong dependence of polarization degree (PD) on energy was found (F. Ursini et al. 2023; A. Di Marco et al. 2023a; M. L. Saade et al. 2024, respectively), while for the *Z*-sources XTE J1701−462, GX 340+0 and GX 5−1, the common trend was a significant change in PD with the transition between the hard and soft state (M. Cocchi et al. 2023; F. La Monaca et al. 2024; S. Fabiani et al. 2024, respectively). Even the upper limits on the PD obtained for GS 1826−238, Ser X-1, GX 3+1, and GX 9+1 (F. Capitanio et al. 2023; F. Ursini et al. 2024; A. Gnarini et al. 2024; A. Tarana et al. 2025, respectively) were used to constrain the inclination of these objects.

It is worth noting that GX 9+9, 4U 1820−303, and 4U 1624−49 showed clear signatures of reflection, whereas GS 1826−238 did not. Reflected emission has been proposed as a key factor in the high polarization observed in these atoll sources, which could explain why GS 1826−238 showed no significant polarization while the three others did. However, Ser X-1, GX 3+1, and GX 9+1, despite also exhibiting reflection features, showed no polarization detection. This has been attributed to the low inclination of these sources.

Moreover, hints for a misalignment between the NS rotation axis and the orbital axis were obtained for Cir X-1 (J. Rankin et al. 2024) and GX 13+1 (A. Bobrikova et al. 2024a, 2024b), although an alternative explanation in terms of eclipse of the scattering region by the outer part of the cold disk also exists (A. Di Marco et al. 2025). Note that both Cir X-1 (T. Oosterbroek et al. 1995; R. E. Shirey et al. 1998) and GX 13+1 (R. S. Schnerr et al. 2003; J. K. Fridriksson et al. 2015) are peculiar cases that display both *Z* and atoll features. Similar behavior has been observed in other sources, with M. Ng et al. (2024) recently reporting that the behavior of 1A 1744−361 is consistent with the idea that atoll and *Z* sources may represent different accretion regimes.

We combine spectroscopic and polarimetric analyses to probe the geometry of a bright atoll source 4U 1735−44. It has a luminosity of around 10% of the Eddington luminosity and is located at a distance of $5.6^{+3.7}_{-2.1}$ kpc (C. A. L. Bailer-Jones et al. 2018). It has an orbital period of 4.564 ± 0.005 hr (R. H. D. Corbet et al. 1989). The inclination of the system is constrained from optical observations at 27°–60° (J. Casares et al. 2006). Analyzing BeppoSAX and XMM-Newton data, B. Mück et al. (2013) obtained an inclination closer to the upper limit of nearly 60°, while R. M. Ludlam et al. (2020), using simultaneous Neutron Star Interior Composition Explorer (NICER) and Nuclear Spectroscopic Telescope Array (NuSTAR) observations, obtained two values, approximately 42° or 57°, concluding that the constraint on inclination is highly model-dependent. The spectrum of 4U 1735−44 has been studied extensively, with a special focus on the reflected component of the emission (see R. M. Ludlam et al. 2020, and references therein). The source is also known to experience regular Type I X-ray bursts (J. van Paradijs et al. 1988; Y.-J. Lei et al. 2013).

Table 1
Log of Observations of 4U 1735−44 Presented in the Paper

Observatory	Dates	ObsID	Instrument	Duration (ks)
IXPE	2024 Aug 31	03004001	DU1	38.8
			DU2	38.9
			DU3	38.9
NICER	2024 Aug 28	7700030101	XTI	1.8
	2024 Aug 29	7700030102	XTI	0 [a]
	2024 Aug 30	7700030103	XTI	0.4
NuSTAR	2024 Aug 31	31001011002	FPMA	33.7
			FPMB	34.2

Note.
[a] The second NICER observation, 7700030102, had no usable data due to known optical light leak issues.

The paper is structured as follows. We describe the observatories used and the data reduction process briefly in Section 2. We present the results of the data analysis in Section 3. We discuss the results and conclude in Section 4.

2. Observations

2.1. IXPE

The Imaging X-ray Polarimetry Explorer (IXPE; M. C. Weisskopf et al. 2022) is the first observatory dedicated to X-ray polarimetry. The mission consists of three identical telescopes, each featuring a gas pixel detector that is sensitive to X-ray polarization in the 2–8 keV energy range (L. Baldini et al. 2021; P. Soffitta et al. 2021). These detectors are positioned at the focal point of the grazing incidence mirror assembly modules. IXPE observed 4U 1735−44 on 2024 August 31 for a total exposure time of about 39 ks for each detector unit (DU). The corresponding ObsIDs and exposure times are given in Table 1.

For the model-independent polarimetric analysis, we processed the data using the IXPEOBSSIM software, version 30.6.3 (L. Baldini et al. 2022). The normalized Stokes *q* and *u* parameters, as well as the PD and polarization angle (PA), were obtained through the `pcube` binning algorithm (F. Kislat et al. 2015).

To carry out the spectral and spectropolarimetric analysis, the source and background regions were selected from the image of each of the three DUs. Source spectra and light curves were extracted from a circular region with a 114″ radius centered on the source, while the background was selected as an annular region centered on the source spanning 180″–240″. We iteratively determined the source extraction radii from 30″ to 180″ in 5″ steps in order to maximize the signal-to-noise ratio (S/N) across the entire IXPE energy range. This approach is similar to that used by E. Piconcelli et al. (2004). Due to the high brightness of this source, the background is negligible (see A. Di Marco et al. 2023b) and was not subtracted. The data reduction was performed, applying the weighted scheme (A. Di Marco et al. 2022). For this analysis, we used the HEASOFT package, version 6.34 (Nasa Heasarc 2014), standard FTOOLS and XSPEC (K. A. Arnaud 1996). The calibration files were obtained from the CALDB version 20240125.

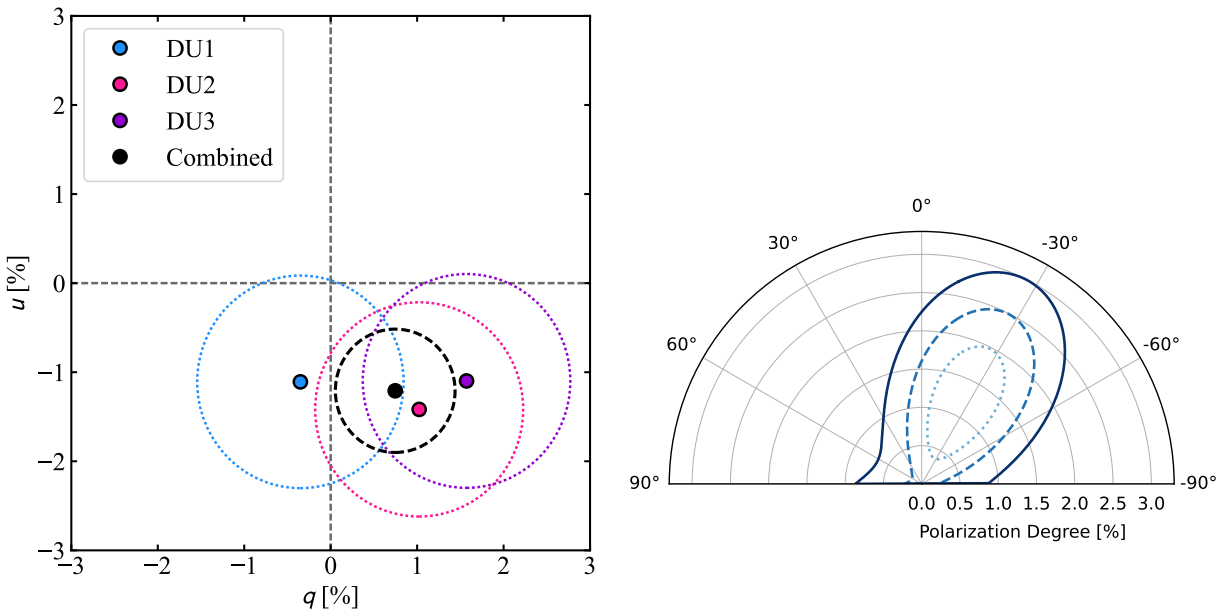

Figure 1. Averaged polarization properties. Left: normalized Stokes q and u parameters in the 2–8 keV band, for the three IXPE DUs and their combination. Errors are provided at 1σ CL. Right: polarization contours in the 2–8 keV band at the 68%, 90% and 99% confidence levels obtained with the `ixpe_protractor` task.

2.2. NuSTAR

NuSTAR (F. A. Harrison et al. 2013) is the first focusing high-energy X-ray mission, operating in the 3–79 keV energy range. It consists of two focal plane modules (FPMA and FPMB) with a spectral resolution of 400 eV (FWHM) at 10 keV.

NuSTAR observed 4U 1735−44 on 2024 August 31 for a total of about 33 ks (see Table 1). We processed the data using NuSTAR Data Analysis Software NUSTARDAS provided under HEASOFT v 6.34. The extraction region radii were determined using the same iterative method as used with IXPE. The extraction radii are 140″ for both focal plane modules (FPMs). The calibration files were obtained from the CALDB version 20240812.

2.3. NICER

NICER (K. C. Gendreau et al. 2016) is mounted on the International Space Station and provides exceptional spectral and timing resolution despite lacking imaging capabilities. Its primary instrument, the X-ray Timing Instrument (XTI), operates in the soft X-ray energy range of 0.2–12 keV.

NICER observed 4U 1735−44 on 2024 August 28, 29, and 30 for a total of 2.2 ks (see Table 1), although the second NICER observation, from August 29, had no usable data due to known optical light leak issues. We processed the data using the NICER Data Analysis Software NICERDAS provided under HEASOFT v 6.34. We used the standard NICER-recommended calibration and filtering tool NICERL2 to produce the clean event files. Standard screening criteria were applied. The calibration files were obtained from the CALDB version 20240206.

3. Data Analysis

3.1. Model-independent Polarimetric Analysis

We performed model-independent polarimetry using the `pcube` tool. The normalized Stokes parameters for the 2–8 keV band are plotted in Figure 1(a), and the polarization contours for PD and PA are shown in Figure 1(b). Combining the data from all three DUs, we obtain a marginally significant (2σ) detection of polarization with PD $= 1.4\% \pm 0.7\%$ and PA $= -29^\circ \pm 14^\circ$, which corresponds to a 3σ upper limit for the PD of 3.5%.

We then analyzed the energy dependence of the polarimetric properties. The results are displayed in Figure 2. The lower panel shows also the MDP99, i.e., the maximum polarization produced by random fluctuations when a true polarization is zero at a confidence level of 99%. A polarization signal is detected at the 99% confidence level (CL) in the 6–7 keV energy bin only with the PD=8.5% ± 2.9% and PA $= -14^\circ \pm 10^\circ$, while the PD is clearly below the MDP99 of ∼3% below 4 keV. This may suggest a possible energy dependence of the PD, but a higher statistical significance is required to draw firm conclusions. We tested alternative binning schemes; however, broader bins did not improve the net significance.

Finally, no evidence for spectral hardness changes is observed, as seen in Figure 3. Thus, we do not expect large variations in polarization over the observation.

3.2. Spectroscopic Analysis

NICER observations happened one day before the IXPE or NuSTAR observations (see Figure 3). Although we attempted a joint spectral fit, the NICER spectrum was not compatible with those from IXPE or NuSTAR, likely due to being in a different spectral state, and no satisfactory fit could be obtained. Hence, we used NuSTAR + IXPE data to perform the spectroscopic analysis.

We began the spectroscopic analysis with a rather simple model. We used the `diskbb` model to simulate the emission coming from the accretion disk and the `comptt` model to simulate the Comptonized emission of the BL/SL region. We chose the spherical geometry of the Comptonizing media. We used the `tbabs` model (J. Wilms et al. 2000) to account for the absorption of the source emission in the interstellar medium. As neither IXPE nor NuSTAR have coverage below 2 keV, we used the HEASARC $N_{\rm H}$ calculator tool based on the survey reported in HI4PI Collaboration et al. (2016).

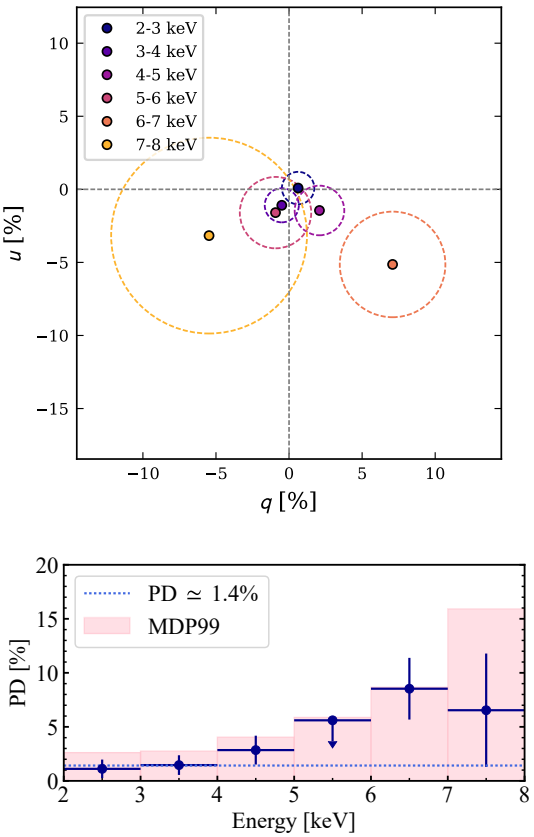

Figure 2. Polarimetric properties as functions of energy. Errors are provided at 1σ CL. Upper panel: normalized Stokes parameters q and u in six energy bands. Lower panel: PD as a function of energy. The 2σ upper limit in the 5–6 keV energy bin is shown.

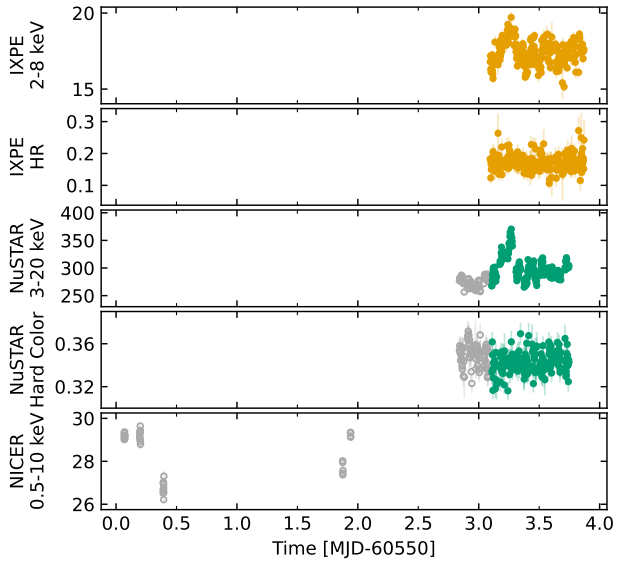

Figure 3. Light curves obtained from IXPE, NuSTAR, and NICER. IXPE hardness ratio (5–8 keV/3–5 keV) and NuSTAR hard color (10–20 keV)/(6–10 keV) are also shown. IXPE observations are shown in orange, simultaneous NuSTAR observations are marked in green and nonsimultaneous observations are marked in gray.

However, the residuals strongly suggested adding a component to account for the reflection of SL/BL emission from the accretion disk. We first added the `gauss` model to simulate the iron line. We obtained a rather broad Gaussian component with $\sigma = 0.88^{+0.06}_{-0.05}$ keV at $E = 6.52^{+0.04}_{-0.05}$ keV, which is an expected energy of the Kα iron line. The results are presented in Table 2, "Model 1" column, and in Figure 4, left panel. We then replaced the `gauss` component with the `relxillNS` (J. A. García et al. 2022) model. Results of this fit are presented in Table 2, "Model 2" column, and in Figure 4, right panel. We note a higher quality of the fit with the `relxill` model.

We tied the blackbody temperature to that of the plasma in the `comptt` model and kept the reflected fraction at -1.0 to model only the reflected component without the blackbody. For the `relxillNS` component, we left the inclination, the inner radius $R_{\rm in}$, the ionization of the accretion disk $\log\xi$, and the normalization of the model to change freely. We fixed the

Table 2
Best-fitting Model Parameters of the Fits to the NuSTAR + IXPE Data

Parameter	Model 1	Model 2
	`tbabs`	
$N_{\rm H}$ (10^{22} cm^{-2})[a]	[0.28]	[0.28]
	`diskbb`	
$kT_{\rm in}$ (keV)	0.79 ± 0.02	$0.90^{+0.04}_{-0.03}$
norm$_{\rm d}$	400 ± 35	240 ± 30
	`comptt`	
kT_0 (keV)	1.11 ± 0.02	$1.34^{+0.07}_{-0.06}$
$kT_{\rm p}$ (keV)	3.01 ± 0.02	2.96 ± 0.02
τ	12.0 ± 0.1	13.6 ± 0.2
norm$_{\rm bb}$	0.27 ± 0.01	0.19 ± 0.01
	`gauss`	
E (keV)	$6.51^{+0.04}_{-0.05}$	⋯
σ (keV)	$0.88^{+0.06}_{-0.05}$	⋯
norm$_g$	0.006 ± 0.001	⋯
	`relxillNS`	
$q_{\rm em}$	⋯	[3.0]
a	⋯	[0.0]
incl (deg)	⋯	39^{+3}_{-2}
$R_{\rm in}$ (ISCO)	⋯	$3.7^{+1.2}_{-0.8}$
$R_{\rm out}$ (grav. r.)	⋯	[400.0]
$kT_{\rm bb}$ (keV)	⋯	[$=kT_{\rm p,comptt}$]
$\log\xi$	⋯	$2.70^{+0.06}_{-0.12}$
$A_{\rm Fe}$	⋯	[1.0]
$\log N$	⋯	[19.0]
norm$_{\rm r}$ (10^{-3})	⋯	1.8 ± 0.2
	Cross-calibration constants	
$C_{\rm DU1-FPMA}$	0.874 ± 0.002	0.873 ± 0.002
$C_{\rm DU2-FPMA}$	0.879 ± 0.002	0.879 ± 0.002
$C_{\rm DU3-FPMA}$	0.857 ± 0.002	0.856 ± 0.002
$C_{\rm FPMB-FPMA}$	0.986 ± 0.001	0.986 ± 0.001
χ^2/degrees of freedom	711/648	679/647
	Photon flux ratios, 2–8 keV	
$F_{\rm diskbb}/F_{\rm tot}$	0.279	0.327
$F_{\rm comptt}/F_{\rm tot}$	0.707	0.476
$F_{\rm gauss}/F_{\rm tot}$	0.014	⋯
$F_{\rm relxillns}/F_{\rm tot}$	⋯	0.197
$F_{\rm tot}$ (erg s^{-1} cm^{-2})	4.0×10^{-9}	4.0×10^{-9}

Notes. Uncertainties are given at a 68% CL. Parameters in square brackets were kept frozen during the fit. Flux is unabsorbed.
[a] This parameter comes from the HEASARC $N_{\rm H}$ calculator tool based on a HI4PI survey (HI4PI Collaboration et al. 2016).

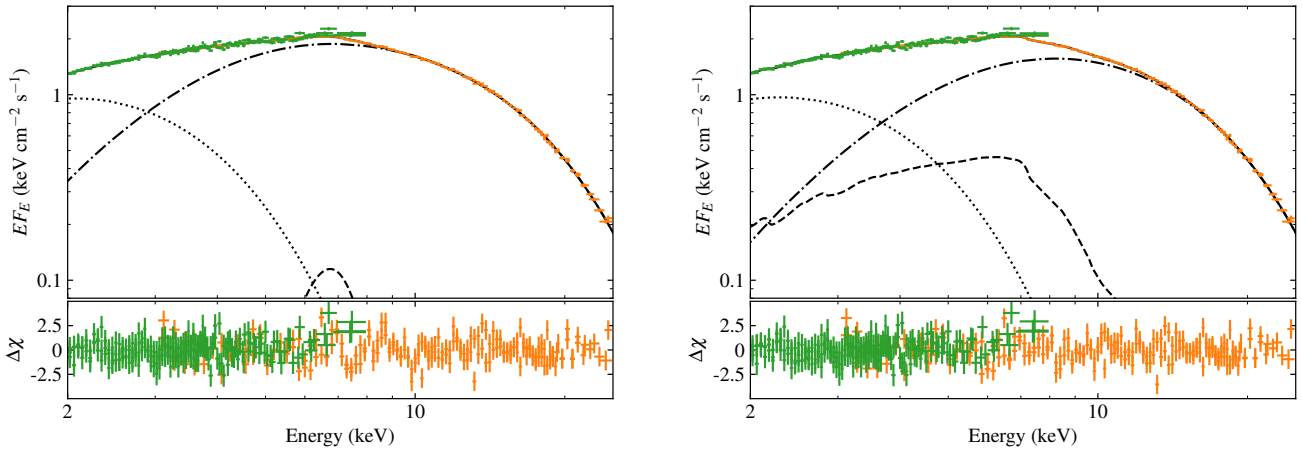

Figure 4. Spectral energy distribution of 4U 1735−44. The IXPE and NuSTAR data are shown with green and orange crosses, respectively. Left panel: fit with the `tbabs*(diskbb+comptt+Gauss)` model. Right panel: fit with the `tbabs*(diskbb+comptt+relxillNS)` model. The lower panels show the fit residuals.

dimensionless spin of the NS at $a = 0.0$ as most NSs in LMXBs have $a \leqslant 0.3$ (D. K. Galloway et al. 2008; J. M. Miller et al. 2011). The lack of data in the low-energy range limited our constraint capabilities. Thus, based on previous spectroscopic analyses of the 4U 1735−44 (R. M. Ludlam et al. 2020), we fixed the emissivity for the coronal flavor models at $q = 3.0$, the density of the accretion disk at $\log N = 19.0$, and the iron abundance at solar level, $A_{\rm Fe} = 1.0$.

The resulting inclination of 39° is lower than the values inferred from previous X-ray observations by B. Mück et al. (2013; ∼ 60°) and R. M. Ludlam et al. (2020; 42°–57°), but is within the broader range of 27°–60° derived from optical observations by J. Casares et al. (2006). Temperatures of the disk $kT_{\rm in}$ and blackbody emission $kT_{\rm bb}$, as well as the Comptonizing media temperature $kT_{\rm p}$, are in agreement with the previous spectroscopic studies of the source (see, e.g., B. Mück et al. 2013; R. M. Ludlam et al. 2020; S. Lavanya et al. 2024). For the inclination obtained from the fit, the disk component normalization corresponds to an inner radius $R_{\rm in,diskbb} \approx$ 10–12 km, depending on the model. According to the correlation between the apparent and true inner radii of the disk given in, for example, A. Kubota et al. (1998), the true inner radius of the disk is only a few km larger than the standard NS radius. Inner radius of the accretion disk from the `relxillNS` model, however, is constrained at $R_{\rm in,relxillNS} = 3.7^{+1.2}_{-0.8}\, R_{\rm ISCO} \approx 45$ km.

3.3. Spectropolarimetric Analysis

To conduct the spectropolarimetric analysis, we used the spectral model presented in Section 3.2 and added the polarimetric model `polconst`. We again fitted NuSTAR + IXPE data and obtained the values of the overall PD = 1.0% ± 0.5% and PA = −25° ± 15° (1σ CL). It is, however, important to note that we can only obtain an upper limit of 2.4% on the PD at 3σ CL, which means that we do not have a strong detection of polarization and the PA is not well constrained. We then attempted to use the `pollin` polarimetric model and fixed the slope on PA at 0. We obtained $\rm PD_{1keV} = -1.3\% \pm 1.2\%$, $\rm PD_{slope} = 0.9 \pm 0.5\%\ keV^{-1}$ and a PA = −29° ± 11° (errors at 1σ CL).[13] We performed an F-test to check if the `pollin` model improved the fitting results significantly, and obtained a probability of 0.082. Hence, we did not see any significant improvement of the fit with `pollin`.

Table 3
Spectropolarimetric Constraints on the Polarization of Different Spectral Components from the NuSTAR + IXPE Data

Component	PD (%)	PA (deg)
overall	1.0 ± 0.5	−25 ± 15
`diskbb`	[1]	54^{+36}_{-39}
`comptt`	[1]	-35^{+60}_{-62}
`relxillNS`	$5.6^{+4.0}_{-2.8}$	-27^{+21}_{-24}
`diskbb`	1.5 ± 1.1	43^{+43}_{-26}
`comptt`	[1]	-31^{+32}_{-34}
`relxillNS`	[5]	-35^{+25}_{-22}
`diskbb`	0.9 ± 0.5	−25 ± 15
`comptt`	$=\rm PD_{diskbb}$	$=\rm PA_{diskbb}$
`gauss`	[0]	[0]

Note. Errors are given at 68% CL. Parameters in square brackets were kept frozen during the fit.

We proceeded with a study of the polarization of each component independently. As we only have a marginal detection of polarization, such a study would not be possible without some artificial constraints. Results of this analysis are presented in Table 3. First, we fixed the polarization of the `diskbb` and `comptt` components to be at PD = 1%, following the expected polarization from these components (V. Loktev et al. 2022; R. Farinelli et al. 2024; A. Bobrikova et al. 2025), and let the polarization of the `relxillNS` component to vary freely. We obtained a $\rm PD_{relxillNS} = 5.6^{+4.0}_{-2.8}\%$ at 1σ CL with the 3σ upper limit of 15%. At 1σ CL, we also obtained constraints on PAs of different components and saw that disk emission seems to be polarized almost orthogonal to the Comptonized component and the reflection. The difference in PA of ∼90° between `diskbb` and other components is consistent with the results of the fit with `pollin` model, which show a flip of the PA by 90° in the IXPE range. We note, however, that the error bars on PA are large for all the components.

[13] The negative value of the PD at 1 keV and a positive PD slope imply a change of the PA by 90° between 1 keV and higher energies, i.e., the actual value of the PA at 1 keV is 63°.

Then, we fixed the relxillNS component polarization at 5% based on our previous results and allowed the diskbb polarization to vary, obtaining a $PD_{diskbb} = 1.5\% \pm 1.1\%$ at 1σ CL with the 3σ upper limit of 5%. We saw again $PA_{relxillNS}$ almost coinciding with PA_{comptt} within 1σ errors, while PA_{diskbb} differs by $\approx 75°$. With this test, we also confirmed that fixing and thawing various components did not have a strong influence on the polarimetric picture. Unfortunately, the statistics did not allow us to perform any further quantitative investigations of the spectro-polarimetric properties using Model 2.

Lastly, we came back to Model 1 from Table 2. As the fluorescent iron line is supposed to be unpolarized, we fixed PD and PA for the gauss component to zero. As we aimed at studying the overall polarization of the source emission, we tied the polarimetric properties of the comptt component to the ones of the diskbb component. We obtained a $PD = 0.9\% \pm 0.5\%$ and $PA = -25° \pm 15°$ at 1σ CL with the 3σ upper limit on the PD of 2.4%. These results are in alignment with the ones obtained from the spectropolarimetric analysis using Model 2.

4. Discussion and Summary

We used IXPE, NuSTAR, and NICER data to investigate the X-ray spectropolarimetric properties of 4U 1735−44. With the model-independent analysis, we obtained a marginal detection of polarization with a PD of $1.4\% \pm 0.7\%$ and PA of $-29° \pm 14°$ with the corresponding 3σ upper limit on the PD of 3.5%. These results, together with the presence of reflection features and a low estimated inclination of 39°, are broadly consistent with the results of other atolls. The spectropolarimetric analysis yielded a $PD = 1.0\% \pm 0.5\%$ and $PA = -25° \pm 15°$ with the corresponding 3σ upper limit on the PD of 2.4%, which is consistent with the values obtained from the pcube polarimetric analysis.

Among other atoll sources, these results are similar to GS 1826−238 (F. Capitanio et al. 2023), Ser X-1 (F. Ursini et al. 2024), GX 3+1 (A. Gnarini et al. 2024), and GX 9+1 (A. Tarana et al. 2025), for which only upper limits could be obtained at 3σ level. The case of 4U 1735−44 appears to be consistent in particular with that of Ser X-1, GX 3+1, and GX 9+1, which, due to their low inclination, showed no polarization detection despite exhibiting reflection features. This suggests 4U 1735−44 may have a similar system geometry and configuration of the Comptonization region.

For future work, longer observations with IXPE should enable tighter constraints on the polarization parameters of 4U 1735−44. In addition to the increased exposure time, applying an event-based maximum likelihood estimation analysis, as described in H. L. Marshall (2021a, 2021b, 2024) and implemented as a Bayesian nested sampling (BNS) method by S. Ravi et al. (2026), can also enhance the detection significance. A longer exposure and stronger polarization signal would shed further light onto the source's behavior.

Acknowledgments

The Imaging X-ray Polarimetry Explorer (IXPE) is a joint US and Italian mission. The US contribution is supported by the National Aeronautics and Space Administration (NASA) and led and managed by its Marshall Space Flight Center (MSFC), with industry partner Ball Aerospace (contract NNM15AA18C). This research used data products provided by the IXPE Team (MSFC, SSDC, INAF, and INFN) and distributed with additional software tools by the High-Energy Astrophysics Science Archive Research Center (HEASARC), at NASA Goddard Space Flight Center (GSFC). This work was partially supported by the Research Council of Finland Centre of Excellence in Neutron-Star Physics (grant 374064). M.A.D.T. acknowledges support from the EDUFI Fellowship and the Johannes Andersen Student Programme at the Nordic Optical Telescope. A.B. was supported by the Finnish Cultural Foundation (grants 002200175 and 00240328). A.G., F.U., S. B., F.C., S.F., G.M., and A.T. acknowledge financial support from the Italian Space Agency (Agenzia Spaziale Italiana, ASI) through the contract ASI-INAF-2022-19-HH.0 and by the Istituto Nazionale di Astrofisica (INAF) through the grant 1.05.23.05.06: "Spin and Geometry in accreting X-ray binaries: The first multi frequency spectro-polarimetric campaign." The Italian contribution was also supported by ASI through contract ASI-OHBI-2022-13-I.0, agreement and ASI-INFN-2017.13-H0, and its Space Science Data Center (SSDC) with agreements ASI-INAF-2022-14-HH.0 and ASI-INFN 2021-43-HH.0, and by the Istituto Nazionale di Fisica Nucleare (INFN) in Italy. A.G. was supported by an appointment to the NASA Postdoctoral Program at the Marshall Space Flight Center (MSFC), administered by Oak Ridge Associated Universities under contract with NASA. M. N. is a Fonds de Recherche du Quebec—Nature et Technologies (FRQNT) postdoctoral fellow. A.S. acknowledges the support of the Jenny and Antti Wihuri Foundation (grant No. 00240331).

Facilities: IXPE, NICER, NuSTAR.

ORCID iDs

María Alejandra Díaz Teodori https://orcid.org/0009-0002-1852-7671
Anna Bobrikova https://orcid.org/0009-0009-3183-9742
Andrea Gnarini https://orcid.org/0000-0002-0642-1135
Francesco Ursini https://orcid.org/0000-0001-9442-7897
Sofia V. Forsblom https://orcid.org/0000-0001-9167-2790
Juri Poutanen https://orcid.org/0000-0002-0983-0049
Alexander Salganik https://orcid.org/0000-0003-2609-8838
Stefano Bianchi https://orcid.org/0000-0002-4622-4240
Fiamma Capitanio https://orcid.org/0000-0002-6384-3027
Massimo Cocchi https://orcid.org/0000-0002-5817-3129
Sergio Fabiani https://orcid.org/0000-0003-1533-0283
Ruben Farinelli https://orcid.org/0000-0003-2212-367X
Philip Kaaret https://orcid.org/0000-0002-3638-0637
Jari J. E. Kajava https://orcid.org/0000-0002-3010-8333
Giorgio Matt https://orcid.org/0000-0002-2152-0916
Mason Ng https://orcid.org/0000-0002-0940-6563
Swati Ravi https://orcid.org/0000-0002-2381-4184
Paolo Soffitta https://orcid.org/0000-0002-7781-4104
Antonella Tarana https://orcid.org/0009-0007-0537-9805
Silvia Zane https://orcid.org/0000-0001-5326-880X

References

Arnaud, K. A. 1996, ASPC, 101, 17
Bahramian, A., & Degenaar, N. 2024, in Low-Mass X-ray Binaries, in Handbook of X-ray and Gamma-ray Astrophysics, ed. C. Bambi & A. Santangelo (Springer), 3657

Bailer-Jones, C. A. L., Rybizki, J., Fouesneau, M., Mantelet, G., & Andrae, R. 2018, AJ, 156, 58
Baldini, L., Barbanera, M., Bellazzini, R., et al. 2021, APh, 133, 102628
Baldini, L., Bucciantini, N., Di Lalla, N., et al. 2022, SoftX, 19, 101194
Bobrikova, A., Di Marco, A., La Monaca, F., et al. 2024a, A&A, 688, A217
Bobrikova, A., Forsblom, S. V., Di Marco, A., et al. 2024b, A&A, 688, A170
Bobrikova, A., Poutanen, J., & Loktev, V. 2025, A&A, 696, A181
Capitanio, F., Fabiani, S., Gnarini, A., et al. 2023, ApJ, 943, 129
Casares, J., Cornelisse, R., Steeghs, D., et al. 2006, MNRAS, 373, 1235
Cocchi, M., Gnarini, A., Fabiani, S., et al. 2023, A&A, 674, L10
Corbet, R. H. D., Smale, A. P., Charles, P. A., et al. 1989, MNRAS, 239, 533
Di Marco, A., Costa, E., Muleri, F., et al. 2022, AJ, 163, 170
Di Marco, A., La Monaca, F., Bobrikova, A., et al. 2025, ApJL, 979, L47
Di Marco, A., La Monaca, F., Poutanen, J., et al. 2023a, ApJL, 953, L22
Di Marco, A., Soffitta, P., Costa, E., et al. 2023b, AJ, 165, 143
Dovčiak, M., Muleri, F., Goosmann, R. W., Karas, V., & Matt, G. 2008, MNRAS, 391, 32
Fabiani, S., Capitanio, F., Iaria, R., et al. 2024, A&A, 684, A137
Farinelli, R., Fabiani, S., Poutanen, J., et al. 2023, MNRAS, 519, 3681
Farinelli, R., Waghmare, A., Ducci, L., & Santangelo, A. 2024, A&A, 684, A62
Fridriksson, J. K., Homan, J., & Remillard, R. A. 2015, ApJ, 809, 52
Galloway, D. K., Muno, M. P., Hartman, J. M., Psaltis, D., & Chakrabarty, D. 2008, ApJS, 179, 360
García, J. A., Dauser, T., Ludlam, R., et al. 2022, ApJ, 926, 13
Gendreau, K. C., Arzoumanian, Z., Adkins, P. W., et al. 2016, SPIE, 9905, 99051H
Gnarini, A., Farinelli, R., Ursini, F., et al. 2024, A&A, 692, A123
Gnarini, A., Ursini, F., Matt, G., et al. 2022, MNRAS, 514, 2561
Harrison, F. A., Craig, W. W., Christensen, F. E., et al. 2013, ApJ, 770, 103
Hasinger, G., & van der Klis, M. 1989, A&A, 225, 79
HI4PI Collaboration, Ben Bekhti, N., Flöer, L., et al. 2016, A&A, 594, A116
Inogamov, N. A., & Sunyaev, R. A. 1999, AstL, 25, 269
Kislat, F., Clark, B., Beilicke, M., & Krawczynski, H. 2015, APh, 68, 45
Kubota, A., Tanaka, Y., Makishima, K., et al. 1998, PASJ, 50, 667
La Monaca, F., Di Marco, A., Ludlam, R. M., et al. 2024, A&A, 691, A253
Lapidus, I. I., & Sunyaev, R. A. 1985, MNRAS, 217, 291
Lavanya, S., Thomas, N. T., Gudennavar, S. B., & Bubbly, S. G. 2024, MNRAS, 534, 2783
Lei, Y.-J., Zhang, H.-T., Zhang, C.-M., et al. 2013, AJ, 146, 60
Lewin, W. H. G., van Paradijs, J., & Taam, R. E. 1993, SSRv, 62, 223
Loktev, V., Veledina, A., & Poutanen, J. 2022, A&A, 660, A25
Ludlam, R. M., Cackett, E. M., García, J. A., et al. 2020, ApJ, 895, 45
Marshall, H. L. 2021a, ApJ, 907, 82
Marshall, H. L. 2021b, AJ, 162, 134
Marshall, H. L. 2024, ApJ, 964, 88
Matt, G. 1993, MNRAS, 260, 663
Miller, J. M., Maitra, D., Cackett, E. M., Bhattacharyya, S., & Strohmayer, T. E. 2011, ApJL, 731, L7
Mück, B., Piraino, S., & Santangelo, A. 2013, A&A, 555, A17
Nasa Heasarc 2014, HEAsoft: Unified Release of FTOOLS and XANADU, Astrophysics Source Code Library, ascl:1408.004
Ng, M., Hughes, A. K., Homan, J., et al. 2024, ApJ, 966, 232
Oosterbroek, T., van der Klis, M., Kuulkers, E., van Paradijs, J., & Lewin, W. H. G. 1995, A&A, 297, 141
Piconcelli, E., Jimenez-Bailón, E., Guainazzi, M., et al. 2004, MNRAS, 351, 161
Popham, R., & Sunyaev, R. 2001, ApJ, 547, 355
Poutanen, J., Nagendra, K. N., & Svensson, R. 1996, MNRAS, 283, 892
Rankin, J., La Monaca, F., Di Marco, A., et al. 2024, ApJL, 961, L8
Ravi, S., Ng, M., Marshall, H. L., & Gnarini, A. 2026, ApJ, 997, 60
Saade, M. L., Kaaret, P., Gnarini, A., et al. 2024, ApJ, 963, 133
Schnerr, R. S., Reerink, T., van der Klis, M., et al. 2003, A&A, 406, 221
Shakura, N. I., & Sunyaev, R. A. 1973, A&A, 24, 337
Shakura, N. I., & Sunyaev, R. A. 1988, AdSpR, 8, 135
Shirey, R. E., Bradt, H. V., Levine, A. M., & Morgan, E. H. 1998, ApJ, 506, 374
Soffitta, P., Baldini, L., Bellazzini, R., et al. 2021, AJ, 162, 208
Suleimanov, V., & Poutanen, J. 2006, MNRAS, 369, 2036
Tarana, A., Capitanio, F., Gnarini, A., et al. 2025, A&A, 698, A245
Ursini, F., Farinelli, R., Gnarini, A., et al. 2023, A&A, 676, A20
Ursini, F., Gnarini, A., Bianchi, S., et al. 2024, A&A, 690, A200
van Paradijs, J., Penninx, W., Lewin, W. H. G., Sztajno, M., & Truemper, J. 1988, A&A, 192, 147
Weisskopf, M. C., Soffitta, P., Baldini, L., et al. 2022, JATIS, 8, 026002
Wilms, J., Allen, A., & McCray, R. 2000, ApJ, 542, 914